SCIENCE CHINA
Information Sciences

• RESEARCH PAPER •

September 2022, Vol. 65 192303:1–192303:10
https://doi.org/10.1007/s11432-021-3329-6

Optical-pulse-coding phase-sensitive OTDR with mismatched filtering

Yongxin LIANG[1], Zinan WANG[1,2*], Shengtao LIN[1], Yuyao WANG[1], Jialin JIANG[1], Zijie QIU[1], Chunye LIU[1] & Yunjiang RAO[1,3]

[1]*Key Lab of Optical Fiber Sensing and Communications, University of Electronic Science and Technology of China, Chengdu* 611731*, China;*
[2]*Center for Information Geoscience, University of Electronic Science and Technology of China, Chengdu* 611731*, China;*
[3]*Research Center for Optical Fiber Sensing, Zhejiang Laboratory, Hangzhou* 310000*, China*

Received 3 May 2021/Revised 28 June 2021/Accepted 23 August 2021/Published online 29 August 2022

Abstract Optical-pulse-coding (OPC) phase-sensitive optical time-domain reflectometry (Φ-OTDR) sends a train of pulses into a fiber, and has high spatial resolution decided by the duration of a subpulse while achieving signal-to-noise ratio (SNR) enhancement. OPC Φ-OTDR with a shorter measurement time is favorable. However, the scan rate, which is the reciprocal of the measurement time, is not easy to optimize. In this paper, mismatched filtering is introduced into OPC Φ-OTDR for the first time, which can reach the theoretical limit of scan rate determined by the fiber length. Also, the initial phase of each subpulse can be set arbitrarily, showing the capacity for controlling the location of interference fading. Although the design of the mismatched filter is based on the least-squares criterion, satisfactory decoding results are obtained, indicating that more advanced mismatched filter designs are worthy of further investigation to achieve higher performance.

Keywords mismatched filtering, phase-sensitive optical time-domain reflectometry, optical fiber sensing, optical pulse coding, least-squares criterion

Citation Liang Y X, Wang Z N, Lin S T, et al. Optical-pulse-coding phase-sensitive OTDR with mismatched filtering. Sci China Inf Sci, 2022, 65(9): 192303, https://doi.org/10.1007/s11432-021-3329-6

1 Introduction

Phase-sensitive optical time-domain reflectometry (Φ-OTDR) is a typical representative of distributed optical fiber sensing systems. Φ-OTDR uses fiber as the sensing medium, and generates Rayleigh backscattering (RBS) light waves for environmental sensing. Due to its high sensitivity and long sensing range, it has already been used in seismic wave detection [1], traffic monitoring [2, 3], acoustic source localization [4,5] and so on. Combined with real-time processing technology [6], Φ-OTDR will play an increasingly important role in sensing.

Optical pulse coding (OPC) is a promising technology in Φ-OTDR to achieve high spatial resolution and sensitivity simultaneously. In 2016, cyclic pulse coding [7] was applied in direct detection Φ-OTDR without quantitative demodulation capability. In this scheme, to reduce interpulse coherence, a distributed feedback (DFB) laser with linewidth greater than 1 MHz is needed as the light source in the 5-km sensing range. Although the scan rate of the system has reached the theoretical limit determined by the fiber length, it is not suitable for coherent detection Φ-OTDR with quantitative demodulation capability. Without orthogonal modulation technologies (such as [8]), the theoretical limit of the scan rate is the reciprocal of the measurement time for one RBS trace acquisition. In OPC Φ-OTDR with coherent detection, the scan rate is still far from the theoretical limit for two reasons. One is the very long coding sequence [9–12]. The other is that several rows of coding sequences are needed to complete a decoding procedure [13–15].

* Corresponding author (email: znwang@uestc.edu.cn)

As for coding with a long sequence, in 2016, the cyclic pseudorandom binary sequence (PRBS) was introduced into coherent detection Φ-OTDR at 2.5-cm spatial resolution in a 500-m fiber [9]. A long coding sequence was needed to obtain a well-behaved spectral distribution, achieving ∼60% of the theoretical scan-rate limit. Then, near perfect periodic autocorrelation (PPA) codes, which were based on biphasic Legendre sequences, were proposed in 2018 with 14.7 cm spatial resolution in a 1-km fiber [10]. Also, due to the long coding sequence in pursuit of a better peak to sidelobe level (PSL), the scan rate was lower than 21% of the theoretical limit. The above schemes have obvious signal-to-noise ratio (SNR) improvement without high-performance external perturbation demodulation results. Higher sensing performance can be realized by shorter PPA codes in a 144-m polarization-maintaining fiber [11], achieving ∼16% of the theoretical scan-rate limit. PPA codes were also used to reduce the relative measurement noise in two-wavelength Φ-OTDR [12], improving the measurement performance of large strain perturbation. The scan rate was only ∼7% of the theoretical limit. In addition to the issue of scan rate, the assistance of a 90° optical hybrid is needed in all the above schemes for decoding, which increases the complexity and cost of the system.

As for coding with several rows of sequences, OPC Φ-OTDR based on Golay codes has had significant advancements in recent years. Bipolar orthogonal complementary Golay codes [13] have a decoding process based on the estimation of a Jones matrix, achieving ∼25% of the theoretical scan-rate limit. A linearized OPC Φ-OTDR with unipolar Golay codes probe pulses can be realized by heterodyne detection and bandpass filtering [14], without necessarily needing a 90° optical hybrid. Furthermore, bipolar-Golay codes probe pulses have been employed in a 10-km fiber at 0.92-m spatial resolution, achieving ∼50% of the theoretical scan-rate limit [15].

To address the scan-rate issue mentioned above, another coding technology called mismatched filtering is investigated here. It has been applied to radar to obtain a better reduction of range sidelobe than matched filtering [16]. This indicates that mismatched filtering can have a satisfactory PSL when a short-coded pulse is used. Additionally, only one coding sequence is needed to complete the decoding procedure. These two characteristics make mismatched filtering a promising technology to improve the scan rate. With years of research and development on mismatched filtering [17, 18], joint optimization designs have become the main trend, one of which is the combination of integrated sidelobe level and PSL [19]. Others are combinations of phase-coded pulses and mismatched filters [20–22].

In this paper, we introduce mismatched filtering into heterodyne detection Φ-OTDR for the first time, which addresses the scan-rate issue. Theory analysis and numerical simulation of mismatched filtering are given first. A modulated coded pulse with a duration of 320 ns is composed of 40 subpulses. The subpulse duration is 8 ns and the intermediate frequency is 625 MHz. Also, the initial phase of each subpulse can be set arbitrarily, which cannot be realized by matched-filtering decoding. According to the results of the reflection at the end of the 1-km fiber in the proof-of-concept experiment, the spatial resolution is close to 32 m without mismatched filtering. After mismatched filtering, the spatial resolution is restored to the submeter level, and it is degraded to 2 m after interference-fading elimination. OPC Φ-OTDR based on mismatched filtering has two characteristics: first, its scan rate determined by the fiber is the highest compared to other OPC Φ-OTDR systems; second, the location of interference fading can be controlled by changing the initial phases of the subpulses. The number of subpulses can also be increased when a longer sensing range or higher SNR is needed.

2 Heterodyne detection Φ-OTDR with mismatched filtering

In this section, we will describe how to implement mismatched filtering to heterodyne detection Φ-OTDR, and then the design of the mismatched filter based on the least-squares criterion is given.

The basic equation of heterodyne detection Φ-OTDR has been discussed fully [23, 24]. The coded RBS trace $y(t)$ can be expressed in the form:

$$y(t) = m(t) * h(t) + n(t), \tag{1}$$

where $*$ is the convolution operation, $m(t)$ is the coded pulse generated by arbitrary waveform generator (AWG) in the experiment, $h(t)$ is the impulse response of heterodyne detection Φ-OTDR, and $n(t)$ is the additive white Gaussian noise (AWGN).

The coded RBS trace $y(t)$ can be decoded by the mismatched filter $m_d(t)$ and can be expressed in the

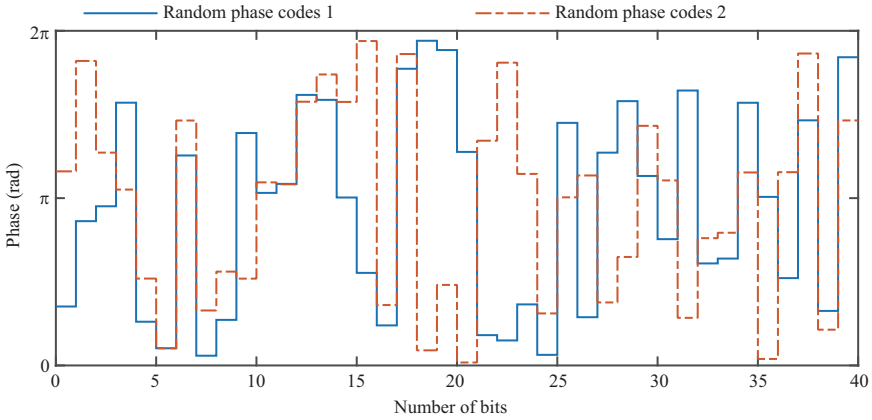

Figure 1 (Color online) The phases of the two random phase codes $\phi_1(n)$.

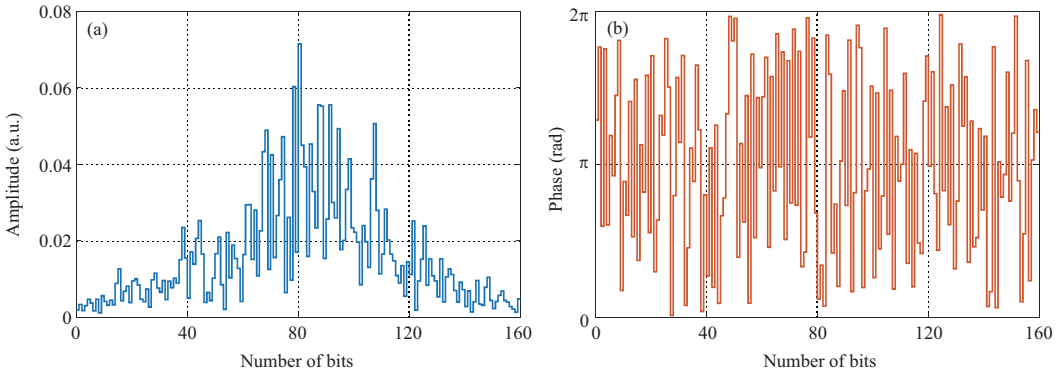

Figure 2 (Color online) (a) The amplitudes and (b) phases of decoding vector $\widehat{u}(n)$ designed by mismatched filtering according to random phase codes 1.

form:

$$y_d(t) = y(t) * m_d(t). \tag{2}$$

Next, we derive the expressions of the coded pulse $m(t)$ and the mismatched filter $m_d(t)$.

As for coding procedure, the coded pulse $m(t)$ with 320 ns width can be expressed in the form:

$$m(t) = m_s(t) * m_c(t), \tag{3}$$

where $m_s(t) = \exp(\mathrm{j}2\pi f_0 t) \cdot \mathrm{rect}(t/T_0)$ is the subpulse with intermediate frequency $f_0 = 625$ MHz and its duration is $T_0 = 8$ ns. The $m_c(t)$ is a sequence constructed from the coding vector $c(n)$. That is,

$$\begin{aligned} m_c(t) &= \sum_{i=1}^{K} [c(i) \cdot \delta(t - (i-1)T_0)], \\ c(i) &= \exp[\mathrm{j}\phi_1(i)], \quad i = 1, 2, \ldots, K, \end{aligned} \tag{4}$$

where $\delta(t)$ is the Dirac delta function, $K = 40$ is the number of subpulses, and $\phi_1(n)$ are the initial phases of subpulses which can be set arbitrarily. Without loss of generality, two groups of random phase codes $\phi_1(n)$ are shown in Figure 1.

As for decoding procedure, the mismatched filter $m_d(t)$ can be expressed as

$$\begin{aligned} m_d(t) &= \sum_{i=1}^{M} [u(i) \cdot \delta(t - (i-1)T_0)], \\ u(i) &= a(i) \exp[\mathrm{j}\phi_2(i)], \quad i = 1, 2, \ldots, M, \end{aligned} \tag{5}$$

where $u(n)$ is the decoding vector, which will be designed by mismatched filtering according to the coding vector $c(n)$, as shown in Figure 2. Different from matched filtering, the length of decoding vector $u(n)$ is

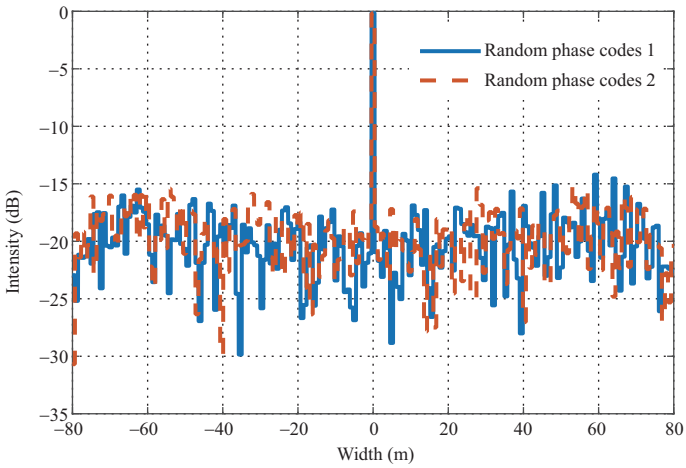

Figure 3 (Color online) Two decoded pulses $m_{dp}(t)$ after mismatched filtering.

generally 2 to 4 times longer than the length of coding vector $c(n)$ [25]. Let the number of M be equal to $4 \cdot K = 160$ here.

In order to figure out how to design the mismatched filter $m_d(t)$, we substitute (1) into (2) and get

$$y_d(t) = m_{dp}(t) * h(t) + n(t) * m_d(t), \tag{6}$$

where

$$m_{dp}(t) = m(t) * m_d(t) = m_s(t) * m_c(t) * m_d(t) \tag{7}$$

is the decoded pulse after mismatched filtering, as shown in Figure 3.

The following part is the detailed derivation of mismatched filtering based on the least-squares criterion, which can be referred to [16, 25]. According to (7) and the convolution properties, we can get

$$m_c(t) * m_d(t) = \sum_{i=1}^{K+M-1} [b(i) \cdot \delta(t - (i-1)T_0)], \tag{8}$$

where vector $b(n)$ is the discrete convolution of coding vector $c(n)$ and decoding vector $u(n)$, and each of its value can be expressed as

$$b(i) = [u(i), u(i-1), \ldots, u(i-K+1)] \begin{bmatrix} c(1) \\ c(2) \\ \cdots \\ c(K) \end{bmatrix}, \quad i = 1, 2, \ldots, K+M-1, \tag{9}$$

where $[u(i), u(i-1), \ldots, u(i-K+1)]$ is a K length vector formed by the decoding vector $u(n)$. It should be noted that, if $i \leqslant 0$, then $u(i) = 0$. After simple derivation, Eq. (9) can be rewritten in the form of matrix:

$$b(n) = \boldsymbol{C}u(n), \tag{10}$$

where vector $b(n) = [b(1), b(2), \ldots, b(K+M-1)]^{\mathrm{T}}$ and decoding vector $u(n) = [u(1), u(2), \ldots, u(M)]^{\mathrm{T}}$. The constraint of vector $b(n)$ is that there is a 1 in the $(M+K)/2$ element and 0 elsewhere. It means that we want only one peak in the center position without any sidelobes in the rest, when coding vector

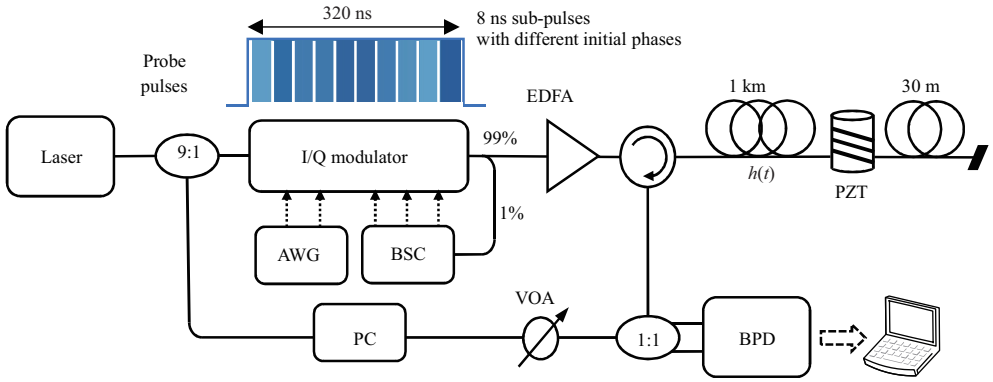

Figure 4 (Color online) Experimental setup of 1-km OPC Φ-OTDR. BSC: bias controller; VOA: variable optical attenuator.

$c(n)$ and decoding vector $u(n)$ are convolved. The matrix

$$\boldsymbol{C}_{(M+K-1)\times M} = \begin{bmatrix} c(1) & 0 & \cdots & 0 \\ \vdots & c(1) & & \vdots \\ c(K) & \vdots & \ddots & 0 \\ 0 & c(K) & & c(1) \\ \vdots & & \ddots & \vdots \\ 0 & \cdots & 0 & c(K) \end{bmatrix} \tag{11}$$

is a Toeplitz matrix formed by the coding vector $c(n)$. Eq. (10) has a least-squares solution, which is

$$\widehat{u}(n) = \left(\boldsymbol{C}^{\mathrm{H}}\boldsymbol{C}\right)^{-1}\boldsymbol{C}^{\mathrm{H}}b(n), \tag{12}$$

where $\widehat{u}(n)$ is the designed decoding vector, and its amplitudes and phases are shown in Figure 2. So far, the design of the mismatched filter has been completed. As mentioned before, substituting $\widehat{u}(n)$ into (5) can get the mismatched filter $m_d(t)$. Then, substituting $m_d(t)$ into (2) can finish the decoding procedure.

Since the coded pulse is based on random phases and the mismatched filter is designed according to the least-squares criterion, the power of sidelobe is relatively obvious, as shown in Figure 3. However, the following experimental analysis finds that the perturbation can be successfully demodulated after fading elimination, meaning that advanced coding and decoding designs based on mismatched filtering, such as [20–22], are worthy of further investigation to obtain higher performance.

3 Experiment and analysis

The experimental setup is shown in Figure 4. The continuous-wave (CW) light from the 1550 nm laser with ultra-narrow linewidth is split into two ports. The 90% port is launched into the I/Q modulator to generate the probe pulse. The AWG generates the coded pulse $m(t)$ according to (3) to drive the I/Q modulator with the predistortion technology [26]. The probe pulse is amplified through the erbium-doped fiber amplifier (EDFA), and then it is launched into a 1-km single-mode optical fiber (SMF). The piezoelectric ceramic transducer (PZT) with 12.3-m fiber is used to generate perturbation.

The 10% port is the local oscillator (LO) light. The polarization controller (PC) is used to modify the polarization state of LO light to get better SNR of RBS traces.

The repeat period of the coded probe pulse is set to 11 μs for 1-km sensing fiber, which means the scan rate reaches the theoretical limit determined by the fiber length. At 2.5 GHz sampling rate, the RBS traces $y(t)$ are generated from the 1.6 GHz balanced photodetector (BPD) after Hilbert transform [27].

The flowchart is shown in Figure 5. They are coding, decoding, and fading elimination. As for coding, the coded pulse $m(t)$ in (3) is a random phase-coded pulse, and its corresponding response is the coded RBS trace $y(t)$ in (1). As for decoding, the width of the decoded pulse $m_{dp}(t)$ can be restored to 8 ns, which is the same as a subpulse width, and its corresponding response is the decoded RBS trace $y_d(t)$ in (6).

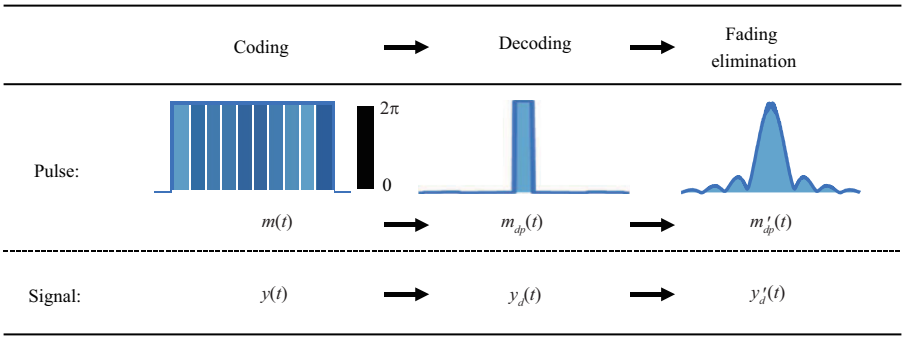

Figure 5 (Color online) The flowchart of the proposed method.

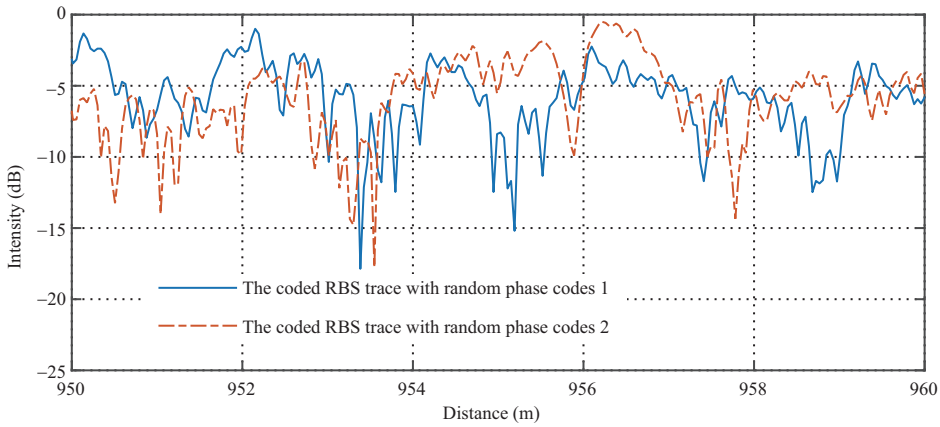

Figure 6 (Color online) The intensities of the two coded RBS traces.

Figure 6 shows the intensity of the coded RBS traces $y(t)$ generated by different modulated coded pulses. It has a different intensity distribution, which indicates the location of interference fading can be controlled intelligently and actively by designating a phase-coded pulse. A similar work is that interference fading can be eliminated by the differential phase shift pulsing technology [28].

Although the spatial resolution can be restored to the half-width length of a subpulse in OPC Φ-OTDR, the existence of interference fading will affect the demodulation of perturbation signal. Fading elimination is of great significance in engineering applications for improving the classification accuracies of perturbation signals with machine learning [29]. Therefore, after mismatched filtering, we use the spectrum extraction and remix (SERM) method to eliminate interference fading [23], which will degrade the spatial resolution.

The parameters of the SERM are as follows. Seven finite impulse response (FIR) bandpass filters with 20-MHz passband and 40-MHz transition bands are used to extract the spectrum. The extracted bandwidth is in the range of 535–595, 555–615, 575–635, 595–655, 615–675, 635–695, and 655–715 MHz, respectively.

Figure 7(a) illustrates the width of the decoded pulses in numerical simulation. The blue dots are the decoded pulse by mismatched filtering, the red line is the decoded pulse after SERM for fading elimination. The 3 dB width of the decoded pulse after SERM is 2 m. Figure 7(b) is the reflection peak at the end of the 1-km fiber. Its 3 dB width is also 2 m, proving that the spatial resolution is 2 m. Their corresponding results in logarithmic coordinates are shown in Figures 7(c) and (d), respectively. It shows that the first sidelobe of the reflection peak is consistent with the numerical simulation.

By launching a train of subpulses, the most obvious advantage of OPC Φ-OTDR is that it brings a large increase in SNR. The 320 ns coded and 8 ns non-coded RBS traces are shown in Figure 8(a). There is about 6.5 dB SNR improvement in intensity. As for the coded RBS trace, the processes are decoding and fading elimination. As for the non-coded RBS trace, only fading elimination is needed. As can be seen from Figure 8(b), after fading elimination, the noise of the decoded RBS trace $y'_d(t)$ is lower than the non-coded RBS trace, which is beneficial for signal demodulation.

The differential phases, which reveal external perturbation in phase demodulation Φ-OTDR, are ex-

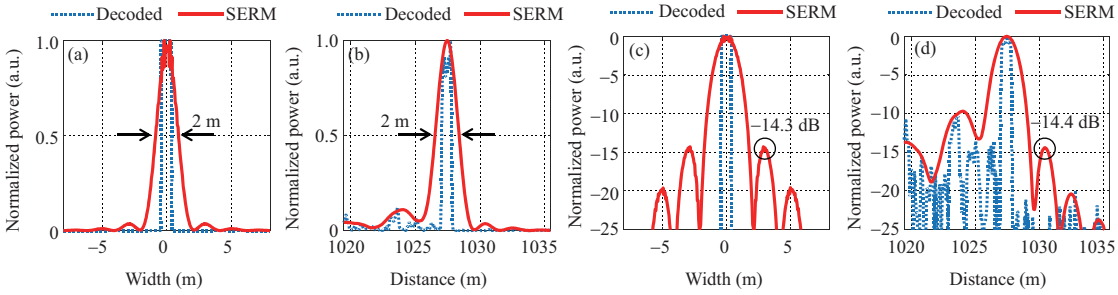

Figure 7 (Color online) (a) The theory of decoded pulses after mismatched filtering (blue dots) and after fading elimination (red solid line). (b) The decoded RBS trace (blue dots) and after fading elimination (red solid line) at the end of the 1-km fiber in the experiment. (c) and (d) are the results of (a) and (b) in logarithmic coordinate, respectively.

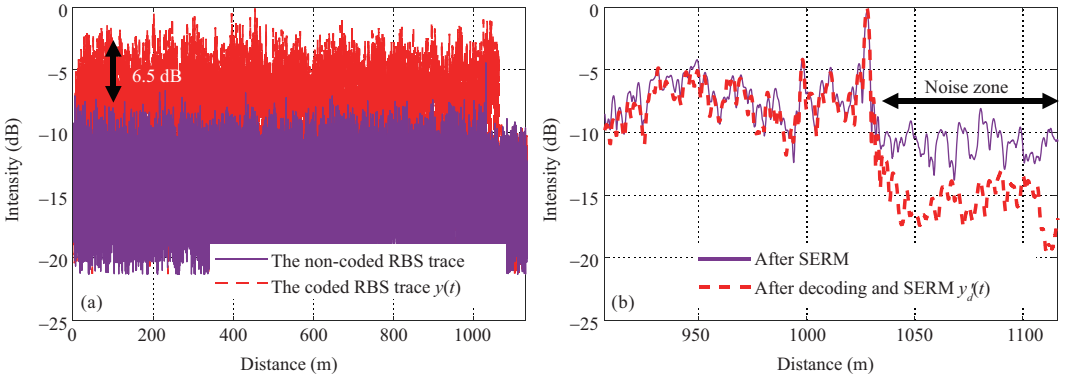

Figure 8 (Color online) Intensity comparisons (a) for the non-coded and coded RBS trace, and (b) their corresponding results after fading elimination.

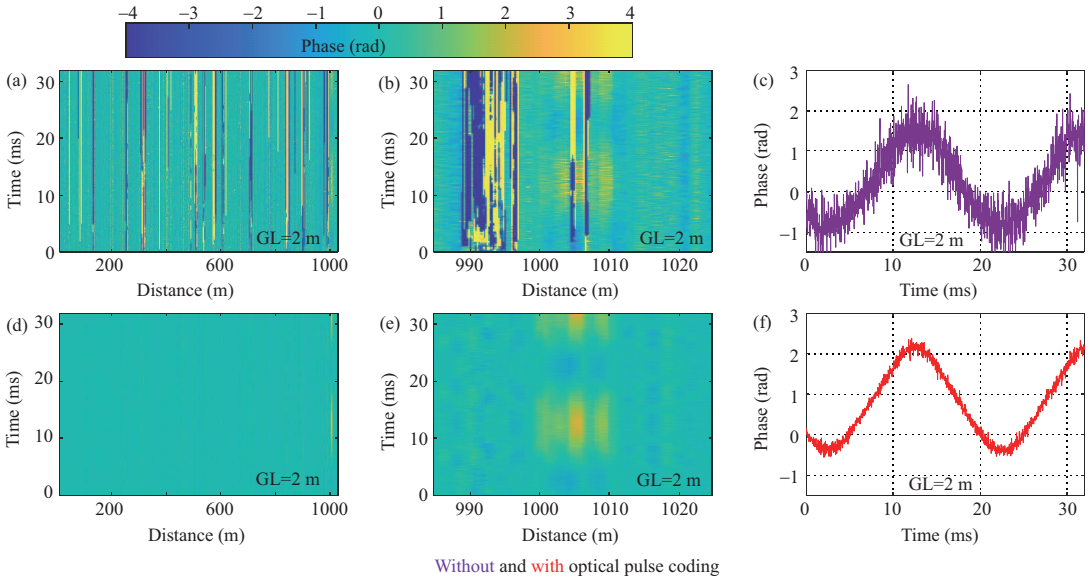

Figure 9 (Color online) After SERM, the differential phases of non-coded RBS traces (a) before the perturbation zone, and (b) in the perturbation zone. (c) The demodulated perturbation signals along the time axis. (d)–(f) are the comparison results for the coded RBS traces. GL: gauge length.

tracted from the decoded RBS traces, which can be referred to [30]. After SERM for fading elimination, the differential phases in the 3-D top view are shown in the first and second columns of Figure 9, and the third column is the demodulated perturbation signals of differential phases at the location of 1006 m where the PZT is located.

The differential phases of the non-coded RBS traces are shown in Figure 9(a). Due to the weak power of RBS traces, the interference fading cannot be eliminated completely. On the contrary, fading is

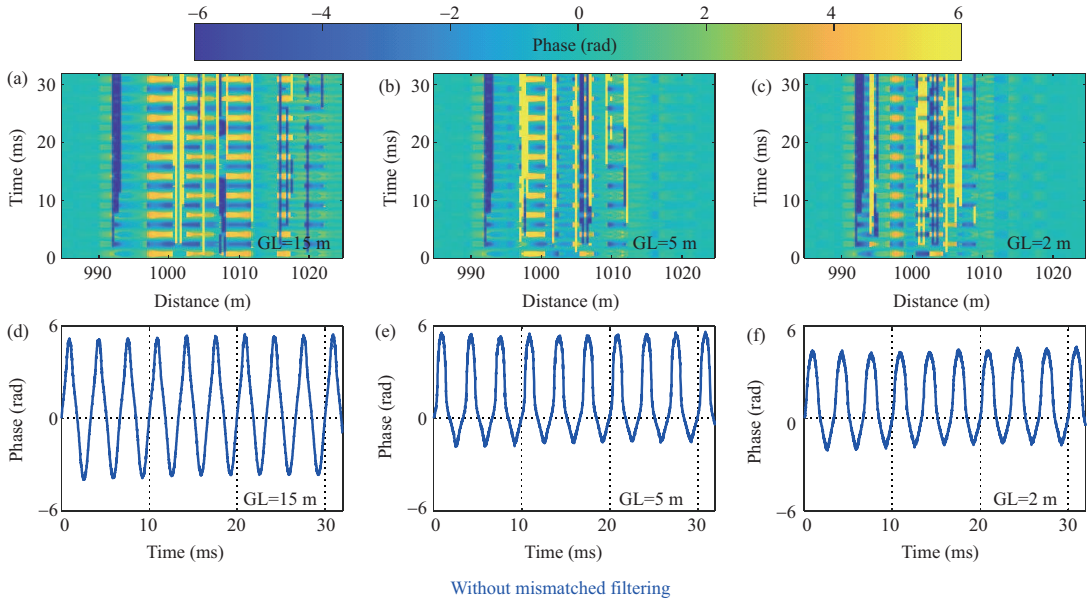

Figure 10 (Color online) After SERM without mismatched filtering, the differential phases with (a) 15-m gauge length, (b) 5-m gauge length, and (c) 2-m gauge length. (d)–(f) are their corresponding demodulated perturbation signals along the time axis.

eliminated completely in the coded differential phases, as shown in Figure 9(d). More detailed observation and comparison results in the perturbation zone are shown in Figures 9(b) and (e). The phase error in Figure 9(b) is no longer observed in Figure 9(e). The SNR of the demodulated perturbation signal shown in Figure 9(f) is 14.2 dB higher than that shown in Figure 9(c).

Without mismatched filtering, the differential phases with 15-m gauge length, 5-m gauge length and 2-m gauge length are disordered, as shown in Figures 10(a)–(c). Similarly, their corresponding demodulated perturbation signals are also distorted, as shown in Figures 10(d)–(f). The demodulation perturbation should be the sine wave at 300 Hz. In this case, Rayleigh scattering responses generated by several subpulses with different time delays will be superimposed together. Serious crosstalk will occur if the phase demodulation is performed, resulting in disordered differential phases and nonlinear demodulated perturbation signals. The results in Figure 10 will be the comparisons for subsequent decoding. If the decoding fails due to the low suppression ratio of the decoded pulse, disordered differential phases will be obtained.

With mismatched filtering, the differential phases with 15-m gauge length, 5-m gauge length and 2-m gauge length are shown in Figures 11(a)–(c). Their corresponding demodulated perturbation signals are shown in Figures 11(d)–(f). The differential phases are no longer disordered, and there is no obvious distortion in these demodulated signals. Compared with the results in Figure 10, mismatched filtering technique is an effective tool for decoding.

The theoretical amplitude of the demodulated perturbation signal is analyzed here. The 0–5 V is applied to 12.3-m PZT whose fiber stretch factor is 0.14 μm/V, corresponding to 0–56.91 nε and 0–4.14 rad phase variation in theory. The amplitude of the demodulated perturbation signal is 4.39 rad in 15-m gauge length, which is consistent with the theoretical value, as shown in Figure 11(d). It can be concluded that the perturbation signal can be recovered correctly by decoding with mismatched filtering. The results show that mismatched filtering can be a critical and effective technology for decoding in OPC Φ-OTDR.

4 Conclusion

A decoding technology using mismatched filtering is introduced into OPC Φ-OTDR for the first time. As a result, the scan rate reaches the theoretical limit determined by the fiber length. With numerical simulation and experimental analysis, the spatial resolution can be restored to the submeter level, and it is degraded to 2 m after interference-fading elimination. In the proof-of-concept experiment, although the coding phases are random, the external perturbation can be demodulated accurately after decoding.

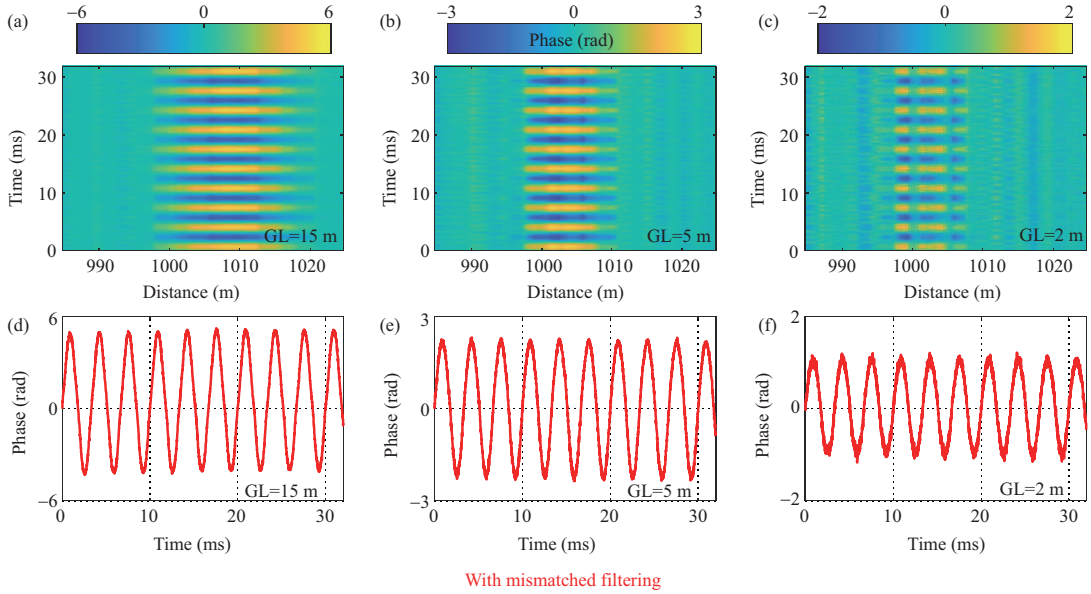

Figure 11 (Color online) After SERM with mismatched filtering, the differential phases with (a) 15-m gauge length, (b) 5-m gauge length, and (c) 2-m gauge length. (d)–(f) are their corresponding demodulated perturbation signals along the time axis.

Besides, the locations of fading are actively controlled by changing the phases of the coded pulse, which provides a new possible solution for interference-fading elimination.

The designed mismatched filter based on the classical criterion of least squares is successfully employed in Φ-OTDR. In further work, advanced design methods [20–22] could make OPC Φ-OTDR become a more powerful system.

Acknowledgements This work was supported by National Natural Science Foundation of China (Grant Nos. 62075030, 61731006), Sichuan Provincial Project for Outstanding Young Scholars in Science and Technology (Grant No. 2020JDJQ0024), and the 111 Project (Grant No. B14039).

References

1 Fernández-Ruiz M R, Soto M A, Williams E F, et al. Distributed acoustic sensing for seismic activity monitoring. APL Photon, 2020, 5: 030901
2 Huang M F, Ji P, Wang T, et al. First field trial of distributed fiber optical sensing and high-speed communication over an operational telecom network. J Lightwave Technol, 2020, 38: 75–81
3 Kowarik S, Hussels M T, Chruscicki S, et al. Fiber optic train monitoring with distributed acoustic sensing: conventional and neural network data analysis. Sensors, 2020, 20: 450
4 Liang J J, Wang Z Y, Lu B, et al. Distributed acoustic sensing for 2D and 3D acoustic source localization. Opt Lett, 2019, 44: 1690–1693
5 Wang Z, Yang J, Gu J, et al. Multi-source aliasing suppression for distributed fiber acoustic sensing with directionally coherent enhancement technology. Opt Lett, 2020, 45: 5672–5675
6 Wang Y, Lv Y, Jin B, et al. Co-processing parallel computation for distributed optical fiber vibration sensing. Appl Sci, 2020, 10: 1747
7 Muanenda Y, Oton C J, Faralli S, et al. A cost-effective distributed acoustic sensor using a commercial off-the-shelf DFB laser and direct detection phase-OTDR. IEEE Photon J, 2016, 8: 1–10
8 Xiong J, Wang Z, Wu Y, et al. Long-distance distributed acoustic sensing utilizing negative frequency band. Opt Express, 2020, 28: 35844–35856
9 Martins H F, Shi K, Thomsen B C, et al. Real time dynamic strain monitoring of optical links using the backreflection of live PSK data. Opt Express, 2016, 24: 22303–35856
10 Shiloh L, Levanon N, Eyal A, et al. Highly-sensitive distributed dynamic strain sensing via perfect periodic coherent codes. In: Proceedings of the 26th International Conference on Optical Fiber Sensors, Lausanne, 2018. TuE25
11 Mompo J J, Shiloh L, Arbel N, et al. Distributed dynamic strain sensing via perfect periodic coherent codes and a polarization diversity receiver. J Lightwave Technol, 2019, 37: 4597–4602
12 Sagues M, Piñeiro E, Cerri E, et al. Two-wavelength phase-sensitive OTDR sensor using perfect periodic correlation codes for measurement range enhancement, noise reduction and fading compensation. Opt Express, 2021, 29: 6021–6035
13 Dorize C, Awwad E, Renaudier J. High Sensitivity φ-OTDR over long distance with polarization multiplexed codes. IEEE Photon Technol Lett, 2019, 31: 1654–1657
14 Wang Z, Zhang B, Xiong J, et al. Distributed acoustic sensing based on pulse-coding phase-sensitive OTDR. IEEE Internet Things J, 2019, 6: 6117–6124
15 Wu Y, Wang Z, Xiong J, et al. Bipolar-coding Φ-OTDR with interference fading elimination and frequency drift compensation. J Lightwave Technol, 2020, 38: 6121–6128
16 Ackroyd M, Ghani F. Optimum mismatched filters for sidelobe suppression. IEEE Trans Aerosp Electron Syst, 1973, AES-9: 214–218
17 Zejak A J, Zentner E, Rapajic P B. Doppler optimised mismatched filters. Electron Lett, 1991, 27: 558–560

18 Blunt S D, Gerlach K. Adaptive pulse compression via MMSE estimation. IEEE Trans Aerosp Electron Syst, 2006, 42: 572–584
19 de Maio A, Piezzo M, Iommelli S, et al. Design of Pareto-optimal radar receive filters. Int J Electron Telecommun, 2011, 57: 477–481
20 Xu L L, Liu H W, Yin K Y, et al. Joint design of phase coded waveform and mismatched filter. In: Proceedings of 2015 IEEE Radar Conference, Johannesburg, 2015. 32–36
21 Tan U, Rabaste O, Adnet C, et al. A sequence-filter joint optimization. In: Proceedings of the 26th European Signal Processing Conference (EUSIPCO), Rome, 2018. 2335–2339
22 Jing Y, Liang J L, Vorobyov S A, et al. Joint design of radar transmit waveform and mismatched filter with low sidelobes. In: Proceedings of the 28th European Signal Processing Conference (EUSIPCO), Amsterdam, 2021. 1936–1940
23 Wu Y, Wang Z, Xiong J, et al. Interference fading elimination with single rectangular pulse in Phi-OTDR. J Lightwave Technol, 2019, 37: 3381–3387
24 Fan X, Yang G, Wang S, et al. Distributed fiber-optic vibration sensing based on phase extraction from optical reflectometry. J Lightwave Technol, 2017, 35: 3281–3288
25 Blunt S D, Mokole E L. Overview of radar waveform diversity. IEEE Aerosp Electron Syst Mag, 2016, 31: 2–42
26 Xiong J, Jiang J, Wu Y, et al. Chirped-pulse coherent-OTDR with predistortion. J Opt, 2018, 20: 034001
27 Jiang J, Wang Z, Wang Z, et al. Coherent Kramers-Kronig receiver for boldsymbol Φ-OTDR. J Lightwave Technol, 2019, 37: 4799–4807
28 Wang X, Lu B, Wang Z, et al. Interference-fading-free Φ-OTDR based on differential phase shift pulsing technology. IEEE Photon Technol Lett, 2019, 31: 39–42
29 Zhang Y X, Zhou T, Ding Z W, et al. Classification of interference-fading suppressed Φ-OTDR signal using optimal peak-seeking and machine learning. In: Proceedings of Optoelectronic Devices and Integration IX, 2020. 6
30 Wang Z, Zhang L, Wang S, et al. Coherent Φ-OTDR based on I/Q demodulation and homodyne detection. Opt Express, 2016, 24: 853–858